frequencies must be identical to those strongly absorbed by the 345 ppmv of CO_2 presently in the atmosphere (*30*). An increase in H_2O in the stratosphere also contributes to an enhanced greenhouse trapping of infrared radiation as an indirect consequence of the CH_4 increase. Finally, the mutually self-limiting nature of the reactions of CH_4 and CO with HO radical make it plausible that the increase in CH_4 mixing ratio is at least partially the result of a progressively lower steady state HO concentration over recent decades (*16, 31*). Predictions of future trends in CH_4 mixing ratios will remain difficult without greatly improved understanding of both its sources and sinks.

REFERENCES AND NOTES

1. D. R. Blake *et al.*, *Geophys. Res. Lett.* **9**, 477 (1982).
2. F. S. Rowland, *Origins Life* **15**, 279 (1985).
3. ———, D. R. Blake, E. W. Mayer, *WMO Spec. Environ. Rep. No. 16, WMO Rep. No. 647* (World Meteorological Organization, Geneva, 1985), p. 33.
4. D. R. Blake and F. S. Rowland, *J. Atmos. Chem.* **4**, 43 (1986).
5. R. A. Rasmussen and M. A. K. Khalil, *J. Geophys. Res.* **86**, 9826 (1981).
6. P. J. Fraser, M. A. K. Khalil, R. A. Rasmussen, A. J. Crawford, *Geophys. Res. Lett.* **8**, 1063 (1981).
7. M. A. K. Khalil and R. A. Rasmussen, *J. Geophys. Res.* **88**, 5131 (1983).
8. R. A. Rasmussen and M. A. K. Khalil, *ibid.* **89**, 11599 (1984).
9. P. J. Fraser *et al.*, *J. Atmos. Chem.* **1**, 125 (1984); M. A. K. Khalil and R. A. Rasmussen, *Antarct. J. U.S.* **19**, 204 (1984).
10. M. A. K. Khalil and R. A. Rasmussen, *Science* **232**, 56 (1986).
11. P. J. Fraser, P. Hyson, R. A. Rasmussen, A. J. Crawford, M. A. K. Khalil, *J. Atmos. Chem.* **4**, 3 (1986).
12. L. P. Steele *et al.*, *ibid.* **5**, 125 (1987).
13. R. C. Robbins, L. A. Cavanagh, L. J. Salas, E. Robinson, *J. Geophys. Res.* **78**, 5341 (1973).
14. H. Craig and C. C. Chou, *Geophys. Res. Lett.* **9**, 1221 (1982); B. Stauffer, G. Fischer, A. Neftel, H. Oeschger, *Science* **229**, 1386 (1985).
15. G. I. Pearman, D. Etheridge, F. deSilva, P. J. Fraser, *Nature (London)* **320**, 248 (1986).
16. C. P. Rinsland, J. S. Levine, T. Miles, *ibid.* **318**, 245 (1985); C. P. Rinsland and J. S. Levine, *ibid.*, p. 250; J. S. Levine, C. P. Rinsland, G. M. Tennille, *ibid.*, p. 254.
17. D. H. Ehhalt, R. J. Zander, R. J. Lamontagne, *J. Geophys. Res.* **88**, 8442 (1983); E. R. Stephens, *ibid.* **90**, 13076 (1985).
18. Y. Makide and F. S. Rowland, *Proc. Natl. Acad. Sci. U.S.A.* **78**, 5933 (1981); E. W. Mayer *et al.*, *ibid.* **79**, 1366 (1982). Our air sample collections have been made since 1977 with a standard 2-liter stainless steel canister equipped with a single stainless steel bellows valve. The canisters are pumped to a vacuum of 10^{-6} torr, transported to remote locations where they are opened to ambient air pressure, and returned to the laboratory for assay by gas chromatography with flame ionization detection. Our measurements are reported for dry air, and are made relative to an NBS standard with an uncertainty of ±1%, corresponding to ±0.02 ppmv. However, because all of the measurements were made relative to the same standard, it is the standard deviation of 0.003 ppmv from intersample comparisons obtained for the standard procedure of alternating measurements of five aliquots each of the individual air sample and of the NBS standard that is appropriate to the study of changes with time. During the past several years, additional smaller (0.4-liter) stainless steel canisters with a single bellows valve have also been used, substantially increasing the number of samples available for CH_4 assay in each collection period. No statistically significant numerical differences have been observed in the CH_4 concentrations found with the 2- and 0.4-liter canisters.
19. D. R. Blake, V. H. Woo, S. C. Tyler, F. S. Rowland, *Geophys. Res. Lett.* **11**, 1211 (1984); F. S. Rowland, S. C. Tyler, Y. Makide, *WMO Spec. Environ. Rep. No. 16, WMO Rep. No. 647* (World Meteorological Organization, Geneva, 1985), p. 13.
20. D. R. Blake and F. S. Rowland, *Nature (London)* **321**, 231 (1986).
21. D. H. Ehhalt and U. Schmidt, *Pure Appl. Geophys.* **116**, 452 (1978).
22. "Atmospheric Ozone 1985", *WMO Global Ozone Res. Monit. Proj. Rep. No. 16* (World Meteorological Organization, Geneva, 1986).
23. E. Matthews and I. Fung, *Global Biogeochem. Cycles* **1**, 61 (1987).
24. E. Robinson, W. L. Bamesburger, F. A. Menzia, A. S. Waylett, S. F. Waylett, *J. Atmos. Chem.* **2**, 65 (1984).
25. The calculated standard deviation of the points from the straight line in Fig. 2 is 0.0025 ppmv, which includes both our errors in routine measurement and the atmospheric sampling error caused by the limited number of samples for each time period. The indicated error bars are graphed as ±0.003 ppmv because of this observed consistency.
26. The increase is estimated from the measured mixing ratios for the two time periods, each ±0.0025 from (*25*).
27. Satellite measurements in the 1980s have confirmed that the summed hydrogen content from H_2O and CH_4 is essentially constant throughout the stratosphere. R. L. Jones *et al.*, *Q. J. R. Meteorol. Soc.* **112**, 1127 (1986).
28. The implicit assumption in such an estimate is that no change has taken place in the average temperature of the tropical tropopause. Some calculations suggest that increasing trace gas concentrations can cause an increase in the tropical tropopause temperature, and this alone could cause stratospheric increases in water vapor mixing ratios. The increasing CH_4 concentrations furnish an avenue for increased H_2O even if the temperature of the tropical tropopause has not been changed.
29. J. C. Farman, B. G. Gardiner, J. D. Shanklin, *Nature (London)* **315**, 207 (1985); R. S. Stolarski *et al.*, *ibid.* **322**, 808 (1986); F. S. Rowland, H. Sato, H. Khwaja, S. M. Elliott, *J. Phys. Chem.* **90**, 1985 (1986); S. Solomon, R. R. Garcia, F. S. Rowland, D. J. Wuebbles, *Nature (London)* **321**, 755 (1986); M. B. McElroy, R. J. Salawitch, S. C. Wofsy, J. A. Logan, *ibid.*, p. 759; L. T. Molina and M. J. Molina, *J. Phys. Chem.* **91**, 433 (1987); D. J. Hofmann, J. W. Harder, S. R. Rolf, J. M. Rosen, *Nature (London)* **326**, 59 (1987).
30. V. Ramanathan, R. J. Cicerone, H. B. Singh, J. T. Kiehl, *J. Geophys. Res.* **90**, 5547 (1985); R. E. Dickinson and R. J. Cicerone, *Nature (London)* **319**, 109 (1986).
31. A. M. Thompson and R. J. Cicerone, *J. Geophys. Res.* **91**, 10853 (1986).

32. Supported by NASA contract No. NAGW-452.

22 October 1987; accepted 7 January 1988

Synchrotron X-ray Diffraction Measurements of Single-Crystal Hydrogen to 26.5 Gigapascals

H. K. MAO, A. P. JEPHCOAT, R. J. HEMLEY, L. W. FINGER, C. S. ZHA, R. M. HAZEN, D. E. COX

The crystal structure and equation of state of solid hydrogen have been determined directly to 26.5 gigapascals at room temperature by new synchrotron x-ray diffraction techniques. Solid hydrogen remains in the hexagonal close-packed structure under these pressure-temperature conditions and exhibits increasing structural anisotropy with pressure. The pressure-volume curve determined from the x-ray data represents the most accurate experimental measurement of the equation of state to date in this pressure range. The results remove the discrepancy between earlier indirect determinations and provide a new experimental constraint on the molecular-to-atomic transition predicted at higher pressures.

THE BEHAVIOR OF SOLID HYDROGEN at high pressures remains a fundamental problem in modern physics. The theoretically predicted high-pressure metallic phase of hydrogen is potentially the simplest metal (*1*) and may display exotic dynamical properties including high-temperature superconductivity (*2*). The properties of hydrogen under extreme pressures also play a central role in modeling the interiors of the giant planets and the early evolution of the solar system (*3*). With the recent steady progress in the maximum pressure attainable in the diamond-anvil cell (*4*), the insulator-to-metal transition in solid hydrogen may well be within range of static compression experiments. Considerable advances have been made in the experimental study of solid hydrogen at high pressure during the last decade (*5–12*). Most recently, vibrational spectroscopic studies indicate that hydrogen remains an insulating molecular solid to ~150 GPa, but the molecular vibron undergoes a pronounced softening above 30 to 50 GPa, which can be interpreted as precursory to the transition to the metallic state (*7*). Direct information on the structure of solid hydrogen at high pressure has been more difficult to obtain than vibrational measurements, and indirect measure-

H. K. Mao, A. P. Jephcoat, R. J. Hemley, L. W. Finger, C. S. Zha, R. M. Hazen, Geophysical Laboratory, Carnegie Institution of Washington, Washington, DC 20008.
D. E. Cox, Department of Physics, Brookhaven National Laboratory, Upton, NY 11973.

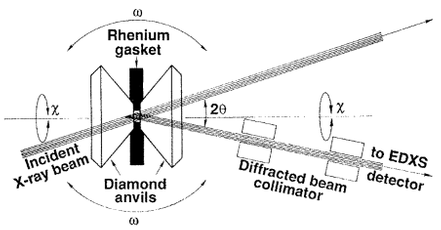

Fig. 1. Schematic diagram of the two-circle system used for single-crystal x-ray diffraction in a diamond-anvil cell with a polychromatic, synchrotron x-ray beam (not to scale). The sample is confined between two 300-μm diamond culets by a rhenium gasket with a hole 50 μm in diameter and 10 μm thick. The diamond-anvil cell is then mounted on a two-circle rotation apparatus equivalent to the χ and ω circle of a four-circle diffractometer. The χ circle consists of a full-circle rotating stage coaxial with the load axis of the diamond anvils and is mounted on a second rotating stage (ω circle) with a vertical axis perpendicular to both the diamond axis and to the plane of incident and diffracted x-ray beams. With a fixed 2θ, a given reflection can be found as a peak in the energy-dispersive x-ray spectrum (EDXS) when the diffraction condition is satisfied for a specific combination of χ and ω. This energy-dispersive system eliminates the need to search with a 2θ circle and reduced the expected 100 hours of searching with a four-circle diffractometer (*14*) to a more practical 2-hour operation. The incident synchrotron x-ray beam is collimated by a pair of adjustable slits, which result in a beam size of the order 10 μm square, and the beam is aligned with the sample in the cell. The collimator on the diffracted beam consists of two slits, one of which is mounted close to the rear diamond anvil to provide the necessary high spatial resolution and to reduce unwanted scattered radiation from the diamonds. The x-ray–induced ruby fluorescence used for determination of the pressure is measured with a microoptical spectrometer system (not shown), which is aligned with the cell on the two-circle apparatus. The measurements were performed on beamline X7A at the National Synchrotron Light Source, Brookhaven National Laboratory.

ments of the equation of state (EOS) of hydrogen at pressures above 2.5 GPa differ significantly (*8–11*). This uncertainty frustrates attempts to test the accuracy of theoretical models of dense hydrogen, including predictions of the insulator-to-metal transition.

Direct determinations of crystal structure and precise equations of state are best obtained by single-crystal x-ray diffration techniques. X-ray diffraction of hydrogen at high pressure, however, presents a great experimental challenge. The x-ray diffraction intensity, which is essentially proportional to the square of atomic number Z, is intrinsically low in hydrogen ($Z = 1$). The surrounding pressure vessel and the diamond anvils comprise higher Z materials and produce a high background signal in any x-ray experiment. Higher pressures in hydrogen have been reached at the expense of significantly smaller sample volumes—approximately 10 nl at 5 GPa, decreasing to 0.1 pl at 150 GPa. Consequently, the intensity of x-ray diffraction from such samples is weak. Previous x-ray diffraction measurements have been performed on large samples under cryogenic conditions near ambient pressure (*13*). Recently, we demonstrated that x-ray diffraction can be used to determine directly the structure of solid hydrogen in a diamond-anvil cell in the gigapascal pressure range with a conventional x-ray source and diffractometer (*14*). The measurements were made at 5.4 GPa and 300 K with a 10-nl hydrogen sample. Successful diffraction measurements at higher pressures proved difficult, however, with a conventional tube x-ray source, because of the required decrease in the workable sample volume at higher pressure. In this case, the strongest diffraction peak with a maximum count rate of 50 sec^{-1} rapidly drops below the background of 15 sec^{-1} under increasing pressure. In addition, the hydrogen single crystals tend to fragment with increasing load in the cell, thereby reducing scattering intensity.

One solution to these problems is provided by the higher x-ray intensities and fine collimation available with synchrotron radiation. In this report we present single-crystal x-ray diffraction measurements as a function of pressure to 26.5 GPa by the use of synchrotron radiation techniques. A new experimental method was designed involving a combination of single-crystal and energy-dispersive diffraction techniques with polychromatic (white) radiation. Energy-dispersive diffraction is employed to significantly reduce the time expended searching for reflections, and a diffracted-beam collimating system is used to achieve high spatial resolution at the sample and to reduce the background signal arising from scattered radiation from the diamond anvils. The apparatus is illustrated schematically in Fig. 1. Hydrogen was compressed in a diamond-anvil high-pressure cell designed for single-crystal x-ray diffraction (*15*). The pressure in the diamond cell was increased above the 300 K freezing point at 5.4 GPa to form a single crystal of hydrogen. The cell was mounted on a two-circle stage as shown in the figure. Pressures were measured by ruby fluorescence excited by the x-ray beam and the quasi-hydrostatic ruby pressure scale was used to calculate the pressure from the wavelength shift of the ruby R_1 band (*16*).

Diffraction patterns at four pressures above the room-temperature freezing point up to a maximum pressure of 26.5 GPa were measured from a single sample (one run). A representative energy-dispersive diffraction pattern at 15 GPa from single-crystal hydrogen is shown in Fig. 2. The crystal structure is observed to be hexagonal close packed (hcp) with space group $P6_3/mmc$, in agreement with previous structure determinations at lower pressures (*13, 14*). The orientation of the crystal was found to shift only slightly with increasing pressure in the lower pressure range, but significantly larger shifts were observed at the two highest pressure points. Although the peak count rate dropped from ~8 sec^{-1} at 15 GPa to 0.05 sec^{-1} at the maximum pressure, the equation of state and lattice parameters could be determined directly over the complete pressure range of the study.

Table 1 summarizes the x-ray diffraction data on solid hydrogen. The measured axial ratio, c/a, where c and a are the lattice constants, is shown in Fig. 3 and appears to decrease with pressure. In both the previous low-temperature measurements (*13*) and lower pressure diamond-anvil study (*14*), an ideal c/a value of 1.633 was found. A decrease in c/a with pressure indicates that the solid is becoming anisotropic. Hence, although there is no indication of orientational ordering [such as that required by a pressure-induced phase transformation to the theoretically predicted, orientationally ordered $Pa3$ cubic structure (*17*)], it is likely that rotation of the H_2 molecules begins to be preferred in the hcp structure at high pressure, with the rotation axis parallel to the c axis.

The four pressure-volume data points obtained from the synchrotron experiment are plotted at 300 K in Fig. 4 together with the

Table 1. Lattice parameters and molar volume of solid hydrogen to 26.5 GPa (300 K), where n_{ref} is the number of reflections used in latice parameter fit. Number in parentheses is uncertainty in last decimal place.

P (GPa)	n_{ref}	a (Å)	c (Å)	c/a	V (cm^3/mol)
5.40(3)*	5	2.659 (2)	4.334 (3)	1.630 (3)	7.992 (2)
10.1 (1)	4	2.5058 (6)	4.074 (1)	1.6260 (7)	6.671 (4)
15.0 (1)	4	2.393 (2)	3.885 (4)	1.624 (2)	5.799 (10)
21.4 (1)	2	2.308 (5)†	3.703 (5)†	1.604 (5)	5.145 (23)
26.5 (1)	2	2.259 (5)†	3.609 (5)†	1.594 (5)	4.791 (22)

*Mo-$K\alpha$ source (*14*). †Uncertainty estimated from the statistics in the EDX pattern.

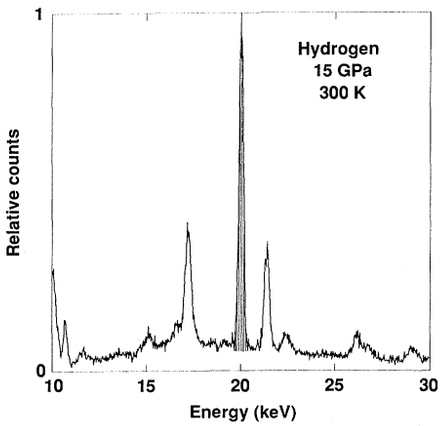

Fig. 2. A representative energy-dispersive x-ray diffraction spectrum for solid hydrogen [(101) reflection] at high pressure.

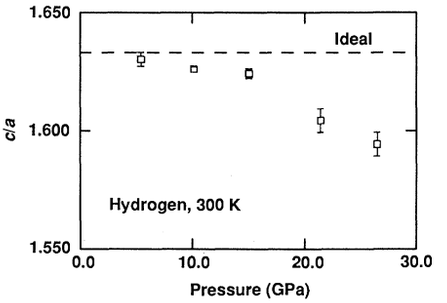

Fig. 3. Pressure dependence of the c/a ratio in solid hydrogen. The dashed line is the ideal value for the hcp structure. For the two highest pressure points, only two reflections were detected. The error bars represent the uncertainty propagated in a least-squares fit to the measured d values.

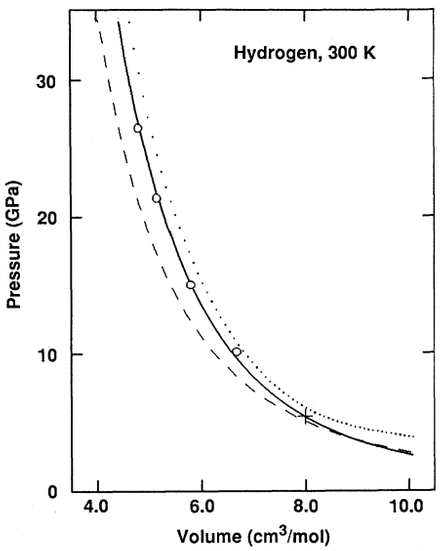

Fig. 4. Pressure-volume data for solid hydrogen at room temperature and the equations of state determined in previous investigations. Symbols: (○), data from this study; (+), data from (*14*); solid line, equation-of-state fit to the present data with K_0 obtained from a fit to low-pressure, low-temperature data of (*20*); dashed line, fit with data from Shimizu *et al.* (*8*); and dotted line, fit with data from van Straaten *et al.* (*9*) corrected to 300 K.

results of the previous study conducted with the conventional x-ray source (*14*). Earlier determinations of the equation of state are also plotted for comparison. The more compressible curve is the room-temperature EOS determined by Shimizu *et al.* (*8*) from Brillouin scattering data. The least compressible curve is the EOS of van Straaten *et al.* (*9*) corrected for the thermal pressure at 300 K with the Mie-Grüneisen model of Hemmes *et al.* (*18*). The two EOS differ by 40% in pressure (10% in density) at 20 GPa. The present data lie at intermediate volumes for all pressures. The solid line represents a fit to the diamond-anvil x-ray diffraction data with a phenomenological equation of state (*19*), in which we have constrained K_0 by earlier low-temperature results to 2.5 GPa (*20*).

The new structural information on solid hydrogen, indicating increasing anisotropy with pressure, provides insight into the discrepancies between previous determinations of the EOS. Shimizu *et al.* (*8*) assumed that solid hydrogen was elastically isotropic in order to calculate density-pressure relation from sound velocities. Van Straaten *et al.* (*9*) assumed an isotropic index of refraction in order to calculate its pressure dependence from the observed fringe shift as a function of the angle of incident light. As stated in their paper, the principal inaccuracy in the EOS arose from the error in index of refraction. The differences between the three curves are at a minimum at 5 GPa and increase with pressure, in accordance with the increasing anisotropy of hydrogen above 5 GPa.

The new EOS for hydrogen can be used to estimate the pressure of the molecular-to-atomic transition predicted at higher pressures. From a comparison between the Gibbs free energy of the molecular phase determined by integration of the extrapolated experimental EOS and the free energies reported recently for possible monatomic phases (*21*), we obtain a lower bound on the transition pressure of 230 GPa. This lower bound, which includes the uncertainty associated with the extrapolation of the experimental EOS, is consistent with recent theoretical treatments of both the molecular and monatomic phases (*21, 22*). A higher compressibility of the molecular phase at high densities is predicted theoretically, a result that shifts the theoretical bounds on the transition pressure to somewhat higher pressures (*21, 22*). This effect may be associated with stabilization of the molecular phase at higher pressures by band overlap, orientational ordering, and vibron-softening but has yet to be determined experimentally.

REFERENCES AND NOTES

1. E. Wigner and H. B. Huntington, *J. Chem. Phys.* **3**, 764 (1935). Numerous calculations of the properties of hydrogen at high density, including the metallic form, have been performed during the past 50 years. The early work has been reviewed by M. Ross and C. Shishkevish, *Molecular and Metallic Hydrogen* (Rand Corporation, Santa Monica, 1977). In addition to the predicted insulator-to-metal transition associated with destruction of the molecular bond, metallization by band overlap in the molecular solid has been predicted [D. E. Ramaker, L. Kumar, F. E. Harris, *Phys. Rev. Lett.* **34**, 812 (1975); C. Friedli and N. W. Ashcroft, *Phys. Rev. B* **16**, 662 (1977)]. Recently several elaborate electronic structure calculations have been performed, most notably the full potential linear augmented–plane-wave (FLAPW) treatment of B. I. Min, H. J. F. Jansen, and A. J. Freeman [*ibid.* **30**, 5076 (1984); *ibid.* **33**, 6383 (1986)], and the quantum Monte Carlo calculations of D. M. Ceperley and B. J. Alder [*ibid.* **36**, 2092 (1987)].
2. N. W. Ashcroft, *Phys. Rev. Lett.* **21**, 1748 (1968); in *Physics of Solids under High Pressure*, J. S. Schilling and R. N. Shelton, Eds. (North-Holland, New York, 1981), p. 155; see also B. I. Min *et al.*, *Phys. Rev. B.* **30**, 5076 (1984).
3. The early work on the role of hydrogen in interior models of the large planets is discussed by V. N. Zharkov and V. P. Trubitsyn [*Physics of Planetary Interiors* (Pachart, Tucson, 1978)]. More recent work is reviewed by W. B. Hubbard [*Planetary Interiors* (Van Nostrand Reinhold, New York, 1984)].
4. H. K. Mao and P. M. Bell, *Science* **200**, 1145 (1978); P. M. Bell, H. K. Mao, K. A. Goettel, *ibid.* **226**, 542 (1984); J. A. Xu, H. K. Mao, P. M. Bell, *ibid.* **232**, 1404 (1986).
5. H. K. Mao and P. M. Bell, *ibid.* **203**, 1004 (1979); V. Diatschenko and C. W. Chu, *ibid.* **212**, 1393 (1981).
6. S. K. Sharma, H. K. Mao, P. M. Bell, *Phys. Rev. Lett.* **44**, 886 (1980); *Carnegie Inst. Washington Yearb.* **79**, 358 (1980); R. J. Wijngaarden, A. Lagendijk, I. F. Silvera, *Phys. Rev. B.* **26**, 4957 (1982); H. K. Mao, J. A. Xu, P. M. Bell, *Carnegie Inst. Washington Yearb.* **82**, 366 (1983).
7. H. K. Mao *et al.*, *Phys. Rev. Lett.* **55**, 99 (1985).
8. H. Shimizu *et al.*, *ibid.* **47**, 128 (1981); H. Shimizu, in *High Pressure in Science and Technology, II* [Materials Research Society Symposium, vol. 22], C. Homan, R. K. MacCrone, E. Whalley, Eds. (North-Holland, New York, 1984), vol. 22, p. 57.
9. J. van Straaten, R. J. Wijngaarden, I. F. Silvera, *Phys. Rev. Lett.* **48**, 97 (1982).
10. W. J. Nellis *et al.*, *Phys. Rev. A* **27**, 608 (1983); M. Ross, F. H. Ree, D. A. Young, *J. Chem. Phys.* **79**, 1487 (1983).
11. V. V. Matveev, I. V. Medvedeva, V. V. Prut, P. A. Suslov, S. A. Shibaev, *JETP Lett.* **39**, 261 (1984).
12. S. N. Ishmaev *et al.*, *Sov. Phys. JETP* **57**, 228 (1983); *ibid.* **62**, 721 (1985).
13. R. L. Mills and A. F. Schuch, *Phys. Rev. Lett.* **15**, 722 (1965); R. L. Mills, A. F. Schuch, D. A. Depatie, *ibid.* **17**, 1131 (1966); A. F. Schuch, R. L. Mills, D. A. Depatie, *Phys. Rev.* **165**, 1032 (1968).
14. R. M. Hazen, H. K. Mao, L. W. Finger, R. J. Hemley, *Phys. Rev. B* **36**, 3944 (1987). A Mo-$K\alpha$ sealed tube x-ray source and automated four-circle diffractometer were used in this study, and a full structure refinement was performed.
15. H. K. Mao and P. M. Bell, *Carnegie Inst. Washington Yearb.* **79**, 409 (1980). The cell was loaded in a pressure vessel containing fluid hydrogen at 0.2 GPa and 300 K. For a description of sample loading techniques, see A. P. Jephcoat, H. K. Mao, P. M. Bell, in *Hydrothermal Experimental Techniques*, G. C. Ulmer and H. L. Barnes, Eds. (Wiley, Interscience, New York, 1987), p. 469.
16. H. K. Mao, J. Xu, P. M. Bell, *J. Geophys. Res.* **91**, 4673 (1986). The pressure dependence of the R_1 ruby fluorescence band obtained with x-ray excitation is identical to that measured with conventional

laser techniques to at least 100 GPa [C. S. Zha *et al.*, *Eos* **67**, 1216 (1986)].
17. I. F. Silvera, *Rev. Mod. Phys.* **52**, 393 (1980); J. van Kranendonk, *Solid Hydrogen* (Plenum, New York, 1983).
18. H. Hemmes, A. Driessen, R. Griessen, *J. Phys. C* **19**, 3571 (1986).
19. We find that the equation-of-state formalism recently developed by P. Vinet *et al.* [*ibid.*, p. L467] provides an excellent representation of our data. In this form of the equation of state, the stress-strain relation is written $H(V) = K_0 \exp\{3/2 [K_0' - 1][1 - (V/V_0)^{1/3}]\}$, where $H(V) = \{(V/V_0)^{2/3}/(3[1 - (V/V_0)^{2/3}])\}P(V)$, and V_0 is the reference volume, K_0 is the bulk modulus, and K_0' is the pressure derivative of the bulk modulus (all at zero pressure). Hence, with V_0 known, K_0 and K_0' may be obtained from the intercept and slope, respectively, from a plot of $\ln[H(V)]$ versus $[1 - (V/V_0)^{2/3}]$. In the present analysis, the diamond-anvil x-ray diffraction data were reduced to $T = 0$ K with a Mie-Grüneisen model for the thermal correction (*18*) and the parameters determined by a least-squares fit. For the fit, it was sufficient to fix the reference volume V_0 and bulk modulus K_0 at their values determined at 4.2 K and to adjust K_0'. With $V_0 = 22.90$ cm^3/mol [for $n - H_2$ at 4.2 K (*17*)] and $K_0 = 0.166$ GPa, K_0' was found to be 7.29 ± 0.02. This parameterization of the $T = 0$ K isotherm is close to that obtained by Vinet *et al.* [*J. Geophys. Res.* **92**, 9319 (1987)], who used only the Anderson and Swenson data to 2.5 GPa (that is, $K_0 = 0.166$ GPa, $K_0' = 7.33$). Further discussion of the equation of state, including a comparison with other functional forms, will be published elsewhere. It is noted that no assumptions with regard to anisotropy of the crystal structure need be made in this analysis.
20. M. S. Anderson and C. A. Swensen, *Phys. Rev. B* **10**, 5184 (1974).
21. We calculate the Gibbs free energy by numerical integration of the $T = 0$ K pressure-volume isotherm calculated from the experimental data and compare the results with interpolated free-energy curves for the static lattice calculated with FLAPW methods [B. I. Min, H. J. F. Jansen, A. J. Freeman, *ibid.* **30**, 5076 (1984); *ibid.* **33**, 6383 (1986)]. The free energy of the molecular phase intersects the free energies of the monatomic phase in the range 230 to 300 GPa, depending on the structure (simple cubic versus face-centered cubic) and neglecting zero-point effects. The most stable structure in the FLAPW calculations for the metallic phase was found to be the hcp, which is close in energy to the simple cubic phase. The FLAPW calculations of the free energies for both molecular and monatomic phase predict a higher transition pressure (400 ± 100 GPa). Although the higher transition pressure suggests that additional stabilization of the molecular phase at high densities is introduced by the theory, significant numerical difficulties were reported in the calculations for this phase. Additional uncertainty in the theoretical calculations may arise from the choice of electron correlation energy functional [A. K. McMahan, in *High-Pressure and Low-Temperature Physics*, C. W. Chu and J. A. Woollam, Eds. (Plenum, New York, 1977), p. 21].
22. D. M. Ceperley and B. J. Alder, *Phys. Rev. B* **36**, 2092 (1987). A transition pressure of 300 ± 40 GPa was obtained with this technique. Although a variety of crystal structures for the molecular phase were examined in this study, the calculations did not include the molecular hcp phase. Orientational ordering was predicted to occur above the pressure range of the present study (at ~100 GPa), consistent with our results.
23. This work was supported by the National Science Foundation under grants EAR-8708127 and EAR-8610068, by the National Aeronautics and Space Administration under grant NAGW214, and by the Carnegie Institution of Washington. Work performed at the National Synchrotron Light Source, Brookhaven National Laboratory, was supported by the Division of Materials Sciences, U.S. Department of Energy, under contract DE-AC02-76CH00016. We thank M. Ross and the referees for constructive reviews of the manuscript.

26 October 1987; accepted 20 January 1988

A Single Receptor Binds Both Insulin-Like Growth Factor II and Mannose-6-Phosphate

RICHARD G. MACDONALD, SUZANNE R. PFEFFER, LISA COUSSENS, MARK A. TEPPER, CAROL M. BROCKLEBANK, JOHN E. MOLE, JACQUELINE K. ANDERSON, ELLSON CHEN, MICHAEL P. CZECH, AXEL ULLRICH

Amino acid sequences deduced from rat complementary DNA clones encoding the insulin-like growth factor II (IGF-II) receptor closely resemble those of the bovine cation-independent mannose-6-phosphate receptor (Man-6-P receptor^{CI}), suggesting they are identical structures. It is also shown that IGF-II receptors are adsorbed by immobilized pentamannosyl-6-phosphate and are specifically eluted with Man-6-P. Furthermore, Man-6-P specifically increases by about two times the apparent affinity of the purified rat placental receptor for ^{125}I-labeled IGF-II. These results indicate that the type II IGF receptor contains cooperative, high-affinity binding sites for both IGF-II and Man-6-P–containing proteins.

THE INSULIN-LIKE GROWTH FACTORS (IGF) I and II exhibit substantial sequence homology to the hormone insulin, which regulates important metabolic effects in humans and other animals (*1*). The IGF peptides mimic insulin action on cellular transport and metabolic pathways and, in many cell types, enhance cell proliferation more potently than insulin (*1*). Three major cell surface receptors bind these peptides with overlapping specificities (*2*). Insulin and IGF-I receptors, denoted as type I, bind their respective ligands with high affinity (dissociation constant, $K_d = 1$ n*M*), but also bind both heterologous peptides with lower affinity. The type I receptors possess heterotetrameric $\alpha_2\beta_2$ subunit structures (*3*) and intrinsic ligand-activated tyrosine kinase activities (*4*) that are essential for their biological functions (*5*). In contrast, the type II IGF receptor preferentially binds IGF-II ($K_d = 1$ n*M*) with higher affinity than IGF-I, but has no affinity for insulin. This receptor consists of a single polypeptide chain (*2, 6*) lacking detectable kinase activity (*7*), and its physiological role is unclear.

In this study of IGF-II receptor function, we obtained amino acid sequences of 14 tryptic peptides derived from the affinity-purified rat placental receptor and synthesized oligonucleotide probes based on two of these sequences (*8*). Several overlapping clones encoding the receptor were isolated from a complementary DNA (cDNA) library prepared from total polyadenylated rat placental RNA (*9*). The composite sequence of 7470 bp contains a 6180-bp open reading frame coding for 2060 amino acids followed by a 1290-bp 3′ noncoding region. The cDNA sequence encodes 11 of the 14 chemically identified receptor peptides, but is still incomplete because the reading frame extends to the extreme 5′ end. Comparison of our deduced rat IGF-II receptor sequence with other proteins contained within a laboratory protein data bank revealed a remarkably high degree of identity (79%) with the recently described sequence of the bovine cation-independent mannose-6-phosphate receptor (Man-6-P receptor^{CI}) (*10*).

Several interesting structural features are revealed upon comparison of the deduced amino acid sequences of the putative cytoplasmic domains of the rat IGF-II receptor, the human IGF-II receptor (*11*), and the bovine Man-6-P receptor^{CI} (*10*). These sequences are 167, 164, and 163 amino acids long, respectively, with an overall 58% sequence identity (Fig. 1). Five regions (Fig. 1, boxed and numbered 1 to 5) show a high degree of sequence conservation among the three species (91% identity compared with 38% for the remaining segments). The five highly conserved regions contain sequences that suggest important functional domains. Region 1, adjacent to the transmembrane sequence, is highly charged as expected for a cytoplasmic stop transfer sequence. Region 2 contains a sequence with the potential to be a substrate for protein kinase C or adenosine 3′,5′-monophosphate (cAMP)–dependent protein kinase, or both. Region 3 is a highly acidic domain analogous to those of several other receptors [for example, the low density lipoprotein (LDL), transferrin, and asialoglycoprotein receptors] that occur at about the same distance from the transmembrane domain (*12*). This region also contains potential tyrosine and serine phospho-

R. G. MacDonald, M. A. Tepper, C. M. Brocklebank, J. E. Mole, J. K. Anderson, M. P. Czech, Department of Biochemistry, University of Massachusetts Medical Center, 55 Lake Avenue North, Worcester, MA 01655.
S. R. Pfeffer, Department of Biochemistry, Stanford University School of Medicine, Stanford, CA 94305.
L. Coussens, E. Chen, A. Ullrich, Department of Developmental Biology, Genentech, Inc., 460 Point San Bruno Boulevard, South San Francisco, CA 94080.